Characterization of Interactions among the Heme Center, Tetrahydrobiopterin, and L-Arginine Binding Sites of Ferric eNOS using Imidazole, Cyanide, and Nitric Oxide as Probes†

Vladimir Berka and Ah-lim Tsai*

Division of Hematology, Department of Internal Medicine, University of Texas Health Science Center at Houston, Houston, Texas 77030

Received December 2, 1999; Revised Manuscript Received May 16, 2000

ABSTRACT: Endothelial nitric oxide synthase (eNOS) is a self-sufficient P450-like enzyme. A P450 reductase domain is tethered to an oxygenase domain containing the heme, the substrate (L-arginine) binding site, and a cofactor, tetrahydrobiopterin (BH_4). This "triad", located at the distal heme pocket, is the center of oxygen activation and enzyme catalysis. To probe the relationships among these three components, we examined the binding kinetics of three different small heme ligands in the presence and absence of either L-arginine, BH_4, or both. Imidazole binding was strictly competitive with L-arginine, indicating a domain overlap. BH_4 had no obvious effect on imidazole binding but slightly increased the k_{on} for L-arginine. L-Arginine decreased the k_{on} and k_{off} for cyanide by two orders, indicating a "kinetic obstruction" mechanism. BH_4 slightly enhanced cyanide binding. Nitric oxide (NO) binding kinetics were more complex. Increasing the L-arginine concentration decreased the NO binding affinity at equilibrium. In both BH_4-abundant and BH_4-deficient eNOS, half of the NO binding sites showed a sizable decrease of the binding rate by L-arginine, with the rate of NO binding at the other half of the sites remaining essentially unaltered by L-arginine, implying that the two heme centers in the eNOS dimer are functionally distinct.

Nitric oxide synthase (NOS)[1] is an unusual self-sufficient P450 cytochrome catalyzing the conversion of L-arginine to nitric oxide (NO) and L-citrulline (*1*−*4*). There are three known isozymes of NOS; the constitutive neuronal NOS (nNOS) and endothelial NOS (eNOS) require calmodulin for enzyme activity, whereas the inducible NOS (iNOS) contains tightly bound calmodulin (*1*−*4*). All three isozymes have a common bidomain structure with the reductase domain containing FAD, FMN, and NADPH binding sites and the oxygenase domain containing the heme center and binding sites for L-arginine and tetrahydrobiopterin (BH_4) (*1*−*4*). The main function of the reductase domain is to provide reducing equivalents to the heme center in the oxygenase domain where the key chemistry of L-arginine conversion occurs. Several X-ray crystallographic structures for the iNOS and eNOS oxygenase domains have been reported recently (*5*−*7*). The overall structure surrounding the heme center is conserved and confirms the proximity between the heme center and the L-arginine and BH_4 binding sites, which together make up an active site "triad". These crystallographic data provide a framework for studying structure−function relationships and the reaction mechanism in NOS.

A useful approach to characterizing the dynamic relationship among the active site triad elements involves kinetic examination of the interaction of NOS with various active site ligands through spectroscopic measurements (*8*−*13*). Data of this sort has been accumulating steadily, providing useful information about subtle differences in ligand binding between NOS isozymes and revealing the influences of L-arginine and BH_4 on heme ligand binding (*14*−*21*). This approach, however, suffers from potential difficulties in data interpretation. NOS samples lacking a full complement of essential cofactors are likely to display heterogeneous ligand binding behavior, and the role of BH_4 as a ligand and/or a cofactor has not been well-defined. Interpretation of ligand binding based on apparent rate constants can be quite difficult, especially in this multiple-ligand binding system. To begin to address these issues, we have established an expression system that produces eNOS with a full complement of heme and flavins and have treated BH_4 as a cofactor instead of as a ligand in the binding studies. Both equilibrium and kinetic binding measurements were performed in the presence and absence of L-arginine, and a mechanistic model was derived that satisfies binding data from both types of binding experiments. We focused on three ligands, imidazole, CN^-, and NO, that interact with ferric eNOS heme in distinct ways. Our data and computer modeling indicate that BH_4, present as a cofactor, has a small effect on binding of these ligands by fixing the heme orientation to give a rigid framework. On the other hand, L-arginine has a strictly

† This work was supported by U. S. Public Health Service Grants GM44911 and GM56818.

* To whom correspondence should be addressed at Division of Hematology, University of Texas Health Science Center, P.O. Box 20708, Houston, TX 77225. E-mail: Ah-lim.Tsai@uth.tmc.edu.

[1] Abbreviations: NOS, nitric oxide synthase; eNOS, endothelial nitric oxide synthase; nNOS, neuronal nitric oxide synthase; BH_4(−) eNOS, BH_4-deficient eNOS; BH_4(+) eNOS, BH_4-reconstituted eNOS; MCD, magnetic circular dichroism; FMN, flavin mononucleotide; FAD, flavin adenine dinucleotide; BH_4, (6*R*)-5,6,7,8-tetrahydro-L-biopterin; 2′- and 3′-AMP, adenosine 2′- and 3′-monophosphate; BCA, bicinchoninic acid; Sf9 cells, *Spodoptera frugiperda* cells.

10.1021/bi992769y CCC: $19.00
Published on Web 07/13/2000

competitive effect on imidazole binding, whereas the effect on CN^- and NO binding is most properly interpreted by an "obstruction" model. The detailed analyses of the ligand interactions in the eNOS oxygenase active site should be useful in understanding the oxygenase catalysis that involves L-arginine, BH_4, and small heme ligand, including oxygen and NO. This information will also help in defining the structural differences not revealed by X-ray crystallography between eNOS and other NOS isozymes.

EXPERIMENTAL PROCEDURES

Materials. L-[2,3,4,5-^{3}H]Arginine and 2′,5′-ADP-Sepharose 4B were purchased from Amersham Pharmacia Biotech. Inc. (*22*). BH_4 was obtained from Schircks Laboratories (Jona, Switzerland). Nitric oxide and argon were from H. P. Gas Products, Inc. (Houston, Texas). NO was further purified by passage through a column packed with KOH pellets. All other chemicals were obtained from Sigma. Sf9 cells were purchased from Pharmingen.

Expression and Purification of Human eNOS. Recombinant human endothelial nitric oxide synthase (eNOS) was prepared using a baculovirus expression system as previously described (*22*−*24*) with slight modifications. For expression of eNOS, Sf9 cells cultured in suspension were infected by recombinant baculoviruses at a multiplicity of infection of 2. Sepiapterin (10 μM) and δ-aminolevulinic acid (100 μM) were added to the culture medium 24 h after infection and hemin chloride (2 μg/mL) was added 48 h after infection. The cells were harvested 72 h postinfection and washed with phosphate buffered saline. Purification of recombinant eNOS was as reported previously (*9*).

Expression and Purification of Bovine eNOS. Bov-eNOSpCW was kindly provided by Dr. Bettie Sue Siler Masters of The University of Texas Health Science Center at San Antonio. The bov-eNOS was expressed in *Escherichia coli* and purified as described by Martásek et al. (*25*). These BH_4(−) eNOS preparations were stored at liquid nitrogen in buffer containing 50 mM Tris, pH 7.5, 10% glycerol, and 0.15 M NaCl. BH_4(+) eNOS was prepared by incubation of the purified BH_4(−) eNOS protein with 500 μM BH_4 for about 2 h during sample concentration by Centriprep (Amicon). Extended incubation with BH_4 did not enhance further BH_4 incorporation but led to heme loss. Excess BH_4 was removed by gel filtration through a 30-cm Bio-Gel P-6DG gel (Bio-Rad) column. Protein fractions were pooled, concentrated by Centriprep 30 (Amicon), and stored in liquid nitrogen in the same buffer as described above for the BH_4(−) eNOS preparations.

Assays of Enzyme Activity. NOS activity was assayed by measuring conversion of L-[^{3}H]arginine to L-[^{3}H]citrulline (*22*, *23*), using a 3-min incubation at 37 °C.

Biopterin Determination. The BH_4 content of purified eNOS was measured using the procedure described previously (*24*).

Protein Determination and Pyridine Hemochromogen Assay. Protein was determined by the BCA (*26*) or modified Lowry (*27*) methods or by quantitation of tryptophan by MCD with L-tryptophan as standard ($A_{282} = 5500\ M^{-1}\ cm^{-1}$) (*28*). The heme content of purified eNOS was measured by pyridine hemochromogen assay (*29*).

Stopped-Flow Experiments. Binding and dissociation rate constants, k_{on} and k_{off}, were determined by kinetic measurements on an Applied Photophysics model SX-18MV stopped-flow instrument with rapid-scan diode-array accessory at 24 °C. Quantitation of ligand binding used the molar absorbance coefficients for ferric eNOS ($\epsilon_{400} = 100\ mM^{-1}\ cm^{-1}$), for the ferric complexes (imidazole, $\epsilon_{432} = 110\ mM^{-1}\ cm^{-1}$; cyanide, $\epsilon_{438} = 87\ mM^{-1}\ cm^{-1}$; and NO, $\epsilon_{442} = 105\ mM^{-1}\ cm^{-1}$) or the difference coefficient for the cyanide complex ($\Delta\epsilon_{442-400} = 97\ mM^{-1}\ cm^{-1}$) and the NO complex ($\Delta\epsilon_{444-398} = 95\ mM^{-1}\ s^{-1}$). For NO binding measurements, the eNOS samples were made anaerobic in a tonometer by five cycles of vacuum and equilibration with argon gas on an anaerobic train. Working NO solutions were prepared by dilution of NO-saturated anaerobic buffer (2 mM at 21 °C) into 0.1 M Tris buffer, pH 7.5, 10% glycerol, and 0.1 M NaCl. Formation of ferric−ligand (cyanide, imidazole, NO) complexes was monitored at the wavelengths indicated in the text. The time courses were analyzed by nonlinear regression to single- or multiple-exponential functions. Estimated k_{on} and k_{off} values were derived from the slope and intercept, respectively, in plots of k_{obs} versus ligand concentrations.

Computer Modeling. The SCoP program (Simulation Resources Inc., Redlands, CA) was used for kinetic simulations and for fittings of single-wavelength kinetic data to the mechanistic model described in Scheme 1. The values for k_1 ($1.0 \times 10^6\ M^{-1}\ s^{-1}$) and k_{-1} ($1.0\ s^{-1}$) for L-arginine binding were determined by binding competition with imidazole (*9*) or assigned based on a K_d of ∼5 μM obtained from static equilibrium titrations for the *E. coli*-expressed eNOS (data not shown). Values of k_2 and k_{-2} were obtained from data from single-ligand kinetic measurements (*9*; and this study). Model A has no floating variables; there are two floating variables in model B (k_3 and k_{-3}), but they are interdependent and constrained by the measured dissociation constant, K_d. Values for k_3 and k_{-3} consistent with the observed kinetic data were obtained by iterative simulations. It is assumed that L-arginine binding rate constants are not influenced by the binding of cyanide or NO, as indicated by the use of k_1 and k_{-1} in both eqs B1 and B4.

Scheme 1: Mechanistic Models Used for Numerical Integration[a]

A. Competition

$$E + A \underset{k_{-1}}{\overset{k_1}{\leftrightarrow}} E\text{-}A \qquad \text{Eq. A1}$$

$$E + B \underset{k_{-2}}{\overset{k_2}{\leftrightarrow}} E\text{-}B \qquad \text{Eq. A.2}$$

B. Obstruction

$$E + A \underset{k_{-1}}{\overset{k_1}{\leftrightarrow}} E\text{-}A \qquad \text{Eq. B1}$$

$$E + C \underset{k_{-2}}{\overset{k_2}{\leftrightarrow}} E\text{-}C \qquad \text{Eq. B2}$$

$$E\text{-}A + C \underset{k_{-3}}{\overset{k_3}{\leftrightarrow}} E\text{-}AC \qquad \text{Eq. B3}$$

$$E\text{-}C + A \underset{k_{-1}}{\overset{k_1}{\leftrightarrow}} E\text{-}AC \qquad \text{Eq. B4}$$

[a] A is L-arg; B is imidazole; C is cyanide or NO; E is BH_4(−) or BH_4(+) eNOS; k_1, k_2, k_3 are the on rate constants; and k_{-1}, k_{-2}, k_{-3} are the off rate constants.

RESULTS

Large-Scale Expression and Purification of Catalytically Active eNOS with a Full Complement of Heme, Flavins, and Abundant BH_4. To define the stoichiometry of the redox cofactors of our eNOS preparation, it was necessary to first resolve the wide variation in the heme extinction coefficient

Table 1: Cofactor Composition of Recombinant Soluble eNOS and Subdomains

sample	stoichiometry (cofactor/monomer) (avg ± SD)				
	heme	FAD	FMN	BH_4	ϵ (mM^{-1} cm^{-1})[e]
eNOS ($n = 5$)[a]	0.52 ± 0.03	0.67 ± 0.04	0.63 ± 0.09	0.19 ± 0.02	123 ± 10
eNOS ($n = 3$)[b]	0.87 ± 0.03	0.76 ± 0.14	0.91 ± 0.10	0.45 ± 0.05	
eNOS ($n = 4$)[c]	0.95 ± 0.04	0.92 ± 0.08	1.01 ± 0.14	0.73 ± 0.03	90 ± 4
oxygenase ($n = 3$)[c]	0.95 ± 0.11	ud[d]	ud	0.55 ± 0.07[e]	91 ± 8
reductase ($n = 2$)	ud	0.85 ± 0.07	1.15 ± 0.07	0.06 ± 0.01	

[a] Sf9 cells: addition of hemin (1 μg/mL) at 48 h post infection. [b] Sf9 cells: addition of 100 μM δ-aminolevulinic acid at 24 h post-infection and 1 μg/mL hemin at 48 h post infection. [c] Sf9 cells: addition of 10 μM sepiapterin, 100 μM δ-aminolevulinic acid at 24 h post-infection, and 1 μg/mL hemin at 48 h post-infection. [d] Undetectable. [e] Heme extinction coefficient.

(values ranging from 71 to 135 mM^{-1} cm^{-1}) in the literature for eNOS samples prepared in different laboratories (*12*, *30*−*32*; and our data) and the related variation in heme content, from 0.4 to 1/monomer (*12*, *30*, *31*).

We have analyzed four different eNOS samples, three different nNOS samples, and one iNOS sample for their heme content and extinction coefficient. Two b-type heme proteins, sperm whale myoglobin and horseradish peroxidase, and two P450s, BM3 and 1A1, were used as standards. Three methods were used for protein determinations as described in Experimental Procedures. The absorbance at 393 nm of L-arginine-treated eNOS, which is fully high-spin eNOS, was used as our reference to determine the molar absorption coefficient. The absorbance at 393 nm was about 3% higher than the absorbance at the 400-nm peak in purified eNOS, which contains both high- and low-spin heme. The flavin components have ~10% contribution at both 393 and 400 nm, as estimated from the spectrum of the isolated reductase domain (data not shown). After correction for the flavin absorbance, the heme extinction of all NOS samples we analyzed ranged from 78 to 97 mM^{-1} cm^{-1}, very similar to published values for typical P450 proteins.

We succeeded in preparing eNOS and its reductase domain with FAD and FMN stoichiometries close to 1 (Table 1) by adding riboflavin to the cell medium (for bacterial expression system only) and supplementing the cell extract with FMN and FAD at the stage of cell breakage. We were also able to further increase the heme content of eNOS and the oxygenase domain to full stoichiometry by adding δ-aminolevulinic acid and hemin to the Sf9 cell medium. As shown in Table 1, four preparations of eNOS purified by ADP-Sepharose affinity chromatography showed a heme content close to unity, a substantial improvement from an earlier value of 0.52 (Table 1). Both FAD and FMN stoichiometries were also close to unity. Surprisingly, even the BH_4 content was significantly increased, to about 0.7/monomer. It thus appears that increasing heme levels in eNOS improves BH_4 incorporation. The eNOS sample expressed from the bacterial system already has a high heme content (~0.8) and a full complement of flavin cofactors, but further treatments used for the Sf9 expression further enhanced the heme stoichiometry to unity and the biopterin content to 0.7 (data not shown). The isolated oxygenase domain from Sf9 expression prepared by the same method showed an optical spectrum significantly improved in quality; the A_{280}/A_{398} ratio was decreased from 2.8 ± 0.5 ($n = 4$) to 1.56. The heme content of this oxygenase is 0.9:1 monomer, significantly better than the values of ~0.5:1 for oxygenase domain samples prepared earlier. Improvement in heme content is also indicated by the decrease of the heme extinction from 122 to 90 mM^{-1} cm^{-1} after we obtained the eNOS preparation with stoichiometric amount of heme (Table 1).

Effect of L*-Arginine on the Binding Kinetics of Imidazole to eNOS.* It was shown earlier that binding of imidazole and L-arginine appears to be competitive to each other due to overlap in binding domains (*9*, *12*, *13*). In our previous published study using baculovirus-expressed eNOS, equilibrium binding competition was performed between imidazole and L-arginine. K_d and K_i values and kinetic imidazole binding was measured at 0.5 mM imidazole and L-arginine varying from 0.05 to 2.5 mM to obtain the on and off rate constants for L-arginine (*9*). To test this competition hypothesis further, eNOS preparations with a full complement of cofactors were used, and computer simulations were performed against the simple competition model (model A) in Scheme 1. Moreover, the effects of both L-arginine and BH_4 were assessed under different experimental conditions.

In the first set of experiments, *E. coli*-expressed eNOS, which is BH_4-deficient [BH_4(−) eNOS], was reacted with a mixture containing 1 mM imidazole and a content of L-arginine varying from 0.025 to 0.5 mM (Figure 1A). At low L-arginine concentrations, i.e., 25 and 50 μM, there was a discernible initial increase of formation of imidazole−ferric eNOS complex as A_{432} increased, followed by a dissociation of imidazole due to L-arginine binding (Figure 1A). When L-arginine concentrations were greater than 0.05 mM, only imidazole dissociation was observed. In the second experiment, *E. coli*-expressed eNOS reconstituted with BH_4 as described in Experimental Procedures, was first preincubated with different amounts of L-arginine and then mixed with 25 mM imidazole in the stopped-flow apparatus to measure the kinetics of imidazole complex formation (Figure 1B). The binding kinetics appears to be exponential, and the equilibrium level of eNOS−imidazole complex decreased with increasing levels of L-arginine. While the appearance of the data in Figure 1, panels A and B, are very different, the observed rate and extent of imidazole complex formation in both data sets were fit exactly by model A using the rate constants obtained previously for individual imidazole and L-arginine binding (Figure 1 and Table 2) (*9*). In the third set of experiments, bacterial [BH_4(−) and BH_4(+)] eNOS (Figure 2) were first treated with 25 μM L-arginine and reacted with various amounts of imidazole. Each reaction showed biphasic kinetics with a rapid increase in A_{432} in less than 50 ms followed by another slower phase that plateaued in a few seconds. This same data (Figure 2) can be fit by a two-exponential function interpreted as a heterogeneity of the eNOS heme. The latter interpretation is, however, very misleading in terms of binding mechanism. In contrast, simulations based on model A and the same set of rate

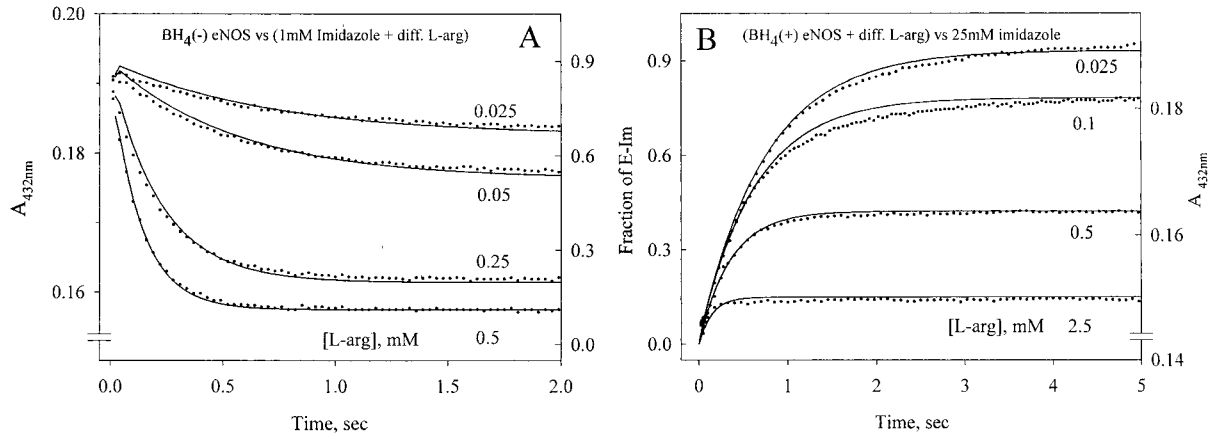

FIGURE 1: Kinetic competition between imidazole and L-arginine. (A) Binding of bacterial eNOS [$BH_4(-)$] (3 μM) with a mixture containing 1 mM imidazole and various amount of L-arginine at 24 °C. Formation of imidazole complex was monitored by $A_{432\ nm}$ (dots). Lines are computer simulations based on mechanistic model A. k_{on} values of 0.8×10^6 and 1.18×10^6 M^{-1} s^{-1} and k_{off} values of 1.2 and 131 s^{-1} were obtained for L-arginine and imidazole, respectively, to reach the best simulation. **(**B) Binding between BH_4-reconstituted bacterial eNOS (3 μM), preincubated with different concentrations of L-arginine, with 25 mM imidazole at 24 °C (dots). Lines are computer simulations using the same parameter values as in panel A. Numbers next to each curve are the concentrations of L-arginine.

Table 2: Kinetics of Imidazole, Cyanide, and NO Binding to eNOS

complex	conditions	obs[a]/sim[b] k_{on} (M^{-1} s^{-1})	obs/sim k_{off} (s^{-1})	obs/sim K_d	stat titra K_d[c]
Fe^{III}−imidazole	−BH_4 −L-arg	1.18×10^6/NA[d]	131/NA	111 μM/NA	
	+BH_4 −L-arg	1.20×10^6/NA	116/NA	108 μM/NA	100 μM
Fe^{III}−CN^-	−BH_4 −L-arg	1.8×10^3/2.0×10^3	22/22	12 mM/11 mM	5.6 mM
	−BH_4 +L-arg	1.36/5.0	1.4/0.2	**1.03** M/**40** mM	15.2 mM
	+BH_4 −L-arg	7.6×10^2/6×10^2	11.5/11.0	15 mM/18 mM	9.6 mM
	+BH_4 +L-arg	1.17/2.0	0.6/0.06	**0.5** M/**30** mM	15.1 mM
Fe^{III}-NO	−BH_4 −L-arg	3.4×10^6/3×10^6	35/50	10.3 μM/17 μM	
first phase ~60%	−BH_4 +L-arg	3.3×10^6/2×10^6	35/40	10.6 μM/20 μM	
second phase ~40%		4.1×10^4/3×10^4	4.3/6.3	104 μM/210 μM	
	+BH_4 −L-arg	3.3×10^6/3×10^6	39/33	11.8 μM/11 μM	
first phase ~70%	+BH_4 +L-arg	3.3×10^6/3×10^6	35/33	10.6 μM/11 μM	
second phase ~30%		NA/1×10^3	1.5/1.5	NA/1.5 mM	

[a] obs: rate constants calculated from secondary plots [b] sim: rate constants from simulation [c] stat titra: values obtained from static titrations [d] NA: not applicable

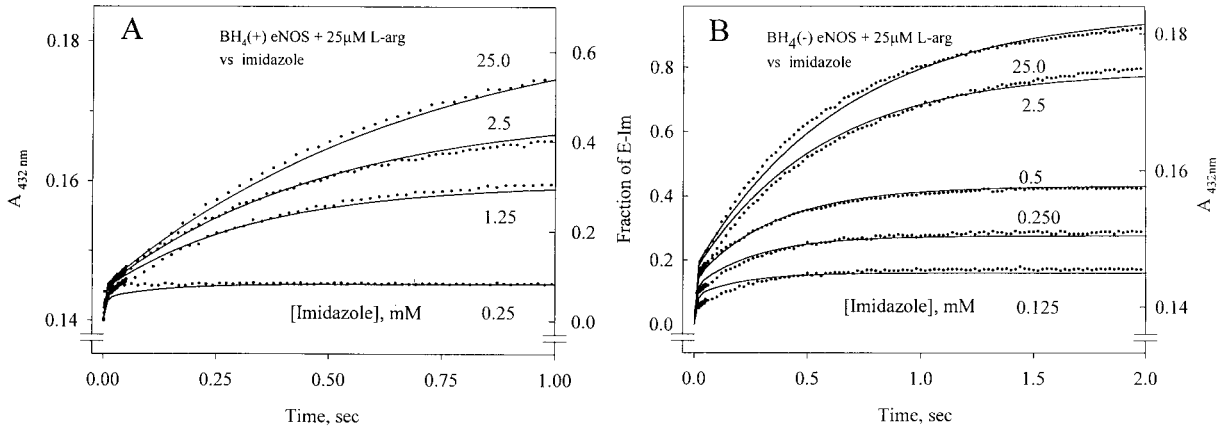

FIGURE 2: Stopped-flow analysis of (eNOS + L-arg)−imidazole complex formation. (A) Bacterial eNOS [$BH_4(+)$] at 3 μM was preincubated with 25 μM of L-arginine and reacted with various amounts of imidazole (dots). Solid lines are computer simulations based on the same model and parameter values used in Figure 1A. (B) Kinetic data for a reaction between 3 μM eNOS [$BH_4(-)$] preincubated with 25 μM of L-arginine and different amount of imidazole (dots). Solid lines are computer simulations. Numbers next to each curve show concentrations of imidazole.

constant values are successful for all three sets of data (lines in Figures 1 and 2). This indicates that the biphasic kinetics in Figure 2 is not due to heme heterogeneity and that BH_4 has minimal influence on the binding behaviors of either imidazole or L-arginine.

Simulations based on model A demonstrated that BH_4 binding enhanced L-arginine binding because a larger k_{on} value for L-arginine had to be used to simulate our binding data that associated with $BH_4(+)$ eNOS than simulation for the $BH_4(-)$ eNOS and accounts for the smaller amount of fast phase observed in Figure 2 (compare panel A vs B). The fast phase is concluded to be the imidazole binding to L-arginine-free eNOS molecules as the on and off rates in this phase match those of free eNOS.

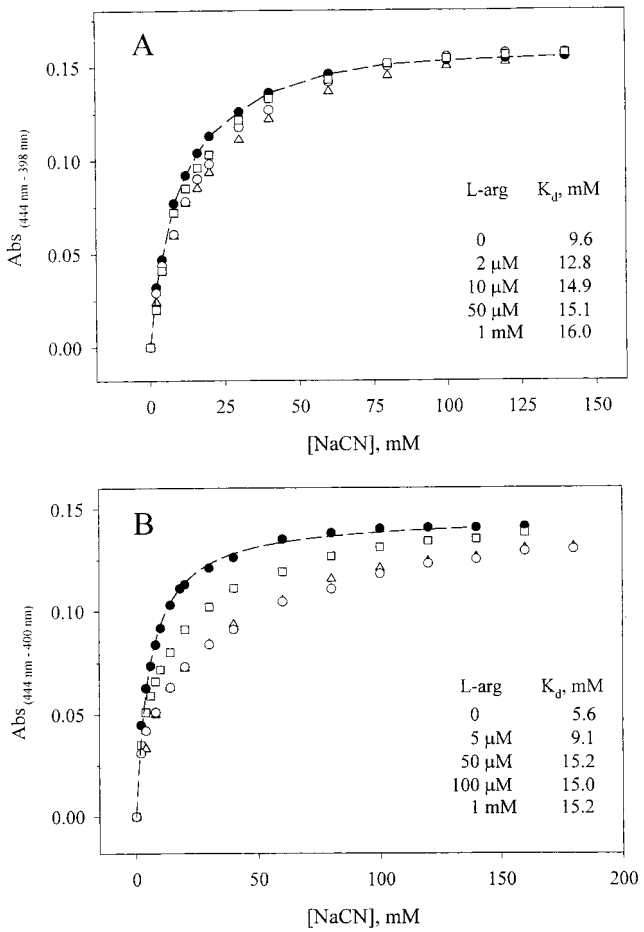

FIGURE 3: Effects of L-arginine on cyanide binding equilibrium with $BH_4(+)$ eNOS and $BH_4(-)$ eNOS. (A) Binding of cyanide to $BH_4(+)$ eNOS (2.5 μM) was monitored by $A_{398-444\ nm}$ in the absence (closed circles) and presence of 2 (open squares), 10 (open circles), and 50 μM (open triangles) L-arginine concentrations. The experiment containing 1 mM L-arginine was essentially superimposable to that containing 50 μM L-arginine. (B) Binding of cyanide to $BH_4(-)$ eNOS containing 0 (closed circles), 5 (open squares), 50 (open circles), 100 μM (open triangles) L-arginine. Titration with 1 mM L-arginine was very similar to that with 100 μM L-arginine. Lines are the hyperbolic fits to the eNOS controls.

Effects of L-Arginine and BH_4 on the Cyanide Binding to eNOS. Equilibrium binding of cyanide to the baculovirus-expressed eNOS [$BH_4(+)$ eNOS] and *E. coli*-expressed eNOS [$BH_4(-)$ eNOS] were conducted using $A_{444-398\ nm}$ and $A_{444-400\ nm}$ as indices, respectively. These titrations were performed at L-arginine concentrations ranging from 0 to 1 mM. For both eNOS controls, the binding isotherms were hyperbolic and the K_d's determined, 9.6 and 5.6 mM, respectively, are similar (Figure 3). Increasing the L-arginine concentration did not change the end point of the titration using either eNOS sample indicating that there is no overlapping in binding domain between L-arginine and cyanide. However, the apparent K_d in the *E. coli* sample appears to be more sensitive to the L-arginine concentration than that of the baculovirus-expressed sample. A 170 and 57% increase in K_d was found for these two eNOS samples, respectively, indicating that the presence of BH_4 attenuated the effect of L-arginine on cyanide binding.

The kinetics of binding of cyanide for the baculovirus-expressed eNOS was also performed in the absence and presence of 25 μM L-arginine using the stopped-flow technique. Without L-arginine, the cyanide binding is accurately monoexponential under pseudo-first-order conditions (Figure 4A). The secondary plot of k_{obs} vs ligand concentrations is linear and yields a second-order on rate constant of 7.6×10^2 M^{-1} s^{-1} from the slope and an off rate constant of 11.5 s^{-1} from the intercept (Figure 4A, inset). These values give a calculated K_d of 15 mM, similar to that obtained from equilibrium binding measurements (Table 2). In the presence of 25 μM L-arginine, cyanide binding slowed substantially although still appeared to be monoexponential (Figure 4B). The apparent k_{on} and k_{off} determined from the secondary plot (Figure 4B, inset) are 1.17 M^{-1} s^{-1} and 0.6 s^{-1}, respectively, giving a calculated K_d of 0.5 M, more than 30 times higher than the L-arginine-free eNOS (Figure 4B and Table 2). This K_d value is also very different from that obtained by the equilibrium titration method (Figure 3A and Table 2). This marked contradiction of K_d values obtained by equilibrium titration and straight secondary plot analysis for the kinetic binding data demands a critical mechanistic assessment.

The competition model (model A in Scheme 1) used for imidazole binding does not apply to cyanide binding kinetics. First of all, the binding equilibrium measurements, particularly for the $BH_4(+)$ eNOS, are not sensitive to L-arginine. Although the apparent K_d for the $BH_4(-)$ eNOS was increased with increasing L-arginine level, the K_d value reaches plateau at 15 mM (Figure 3). Furthermore, the end point of ferric heme cyanide complex formation in equilibrium binding measurements remained practically constant regardless of the L-arginine concentration (Figure 3). To interpret these data, we propose that binding of L-arginine impedes the cyanide ligand in both the on and off directions, but there is no binding domain overlap with the L-arginine binding site. Thus CN^- binding to the eNOS heme will show the same final level of binding complex either with or without L-arginine in the binding system. This simple obstruction model shown in Scheme 1 (model B) successfully simulated the cyanide binding data in the presence of L-arginine (solid lines in Figure 4B) by decreasing the values of k_2 and k_{-2} (600 M^{-1} s^{-1} and 11.0 s^{-1}, respectively) to k_3 and k_{-3} (2.0 M^{-1} s^{-1} and 0.06 s^{-1}, respectively) when L-arginine is introduced (Table 2). These are ~300- and ~180-fold changes, respectively.

The cyanide binding kinetics of *E. coli*-expressed eNOS [$BH_4(-)$] are very similar to those of the baculovirus-expressed eNOS [$BH_4(+)$]. The control experiments without L-arginine treatment also exhibit homogeneous kinetic behavior (Figure 5A) with a linear dependence of k_{obs} on cyanide concentrations (Figure 5A, inset). The second-order association rate constant is 1.8×10^3 M^{-1} s^{-1}, and the dissociation rate constant is 22 s^{-1}, leading to a K_d of 12 mM. This calculated K_d is also close to that obtained from an optical equilibrium titration study (Figure 3 and Table 2). With 50 μM L-arginine present, the cyanide binding kinetics became clearly biphasic (Figure 5B). The fast phase that contributed ~10−20% of the total observed change had a rate close to that of the untreated eNOS, whereas the dominant slow-phase showed a greatly decreased rate. The secondary plot of k_{obs} for the slow phase and cyanide concentration was linear and yielded an apparent k_{on} of 1.36 M^{-1} s^{-1} and an apparent k_{off} of 1.4 s^{-1} (Figure 5B, inset). The calculated K_d is thus 1.03 M, about 85-fold higher than that obtained from eNOS binding kinetics without L-arginine

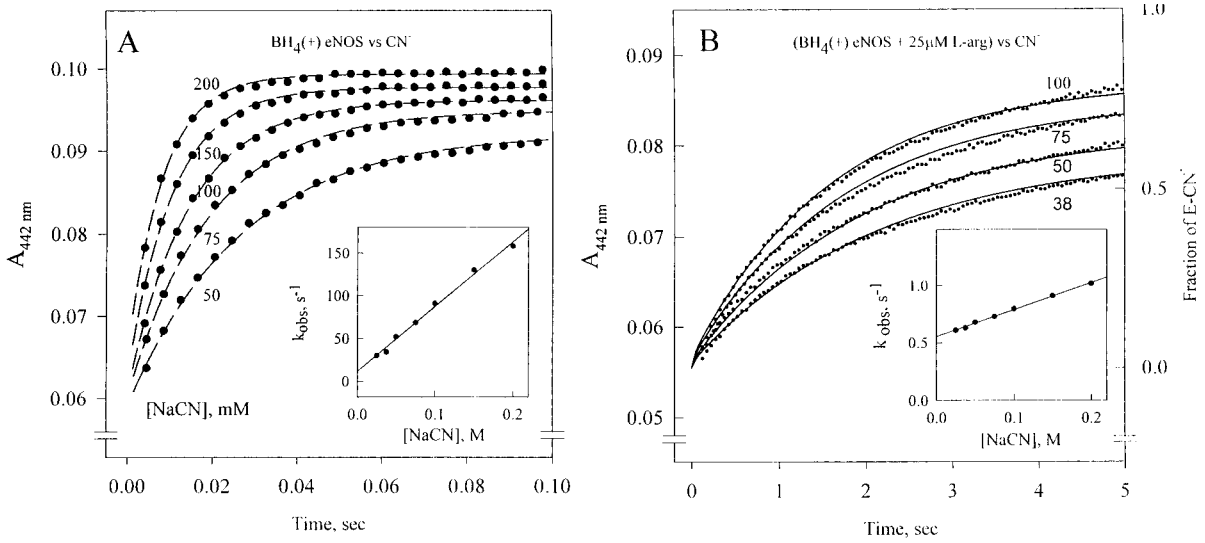

FIGURE 4: Kinetics of $BH_4(+)$ eNOS reaction with cyanide. (A) eNOS at 2 μM was reacted with various levels of cyanide (indicated in millimolar next to each kinetic curve) at 24 °C. Kinetics of absorbance changes at 442 nm (closed circles) were fitted to a single-exponential function (dash lines) to obtain the k_{obs} values. Inset, secondary plot to determine the binding rate constants for cyanide binding to baculovirus eNOS. (B) Kinetics of reaction between $BH_4(+)$ eNOS, preincubated with 25 μM L-arginine, and cyanide. Solid lines are computer simulations based on model B described in Scheme 1. Inset: secondary plot for baculovirus eNOS preincubated with 25 μM L-arginine. Numbers next to each line are the millimolar concentrations of cyanide.

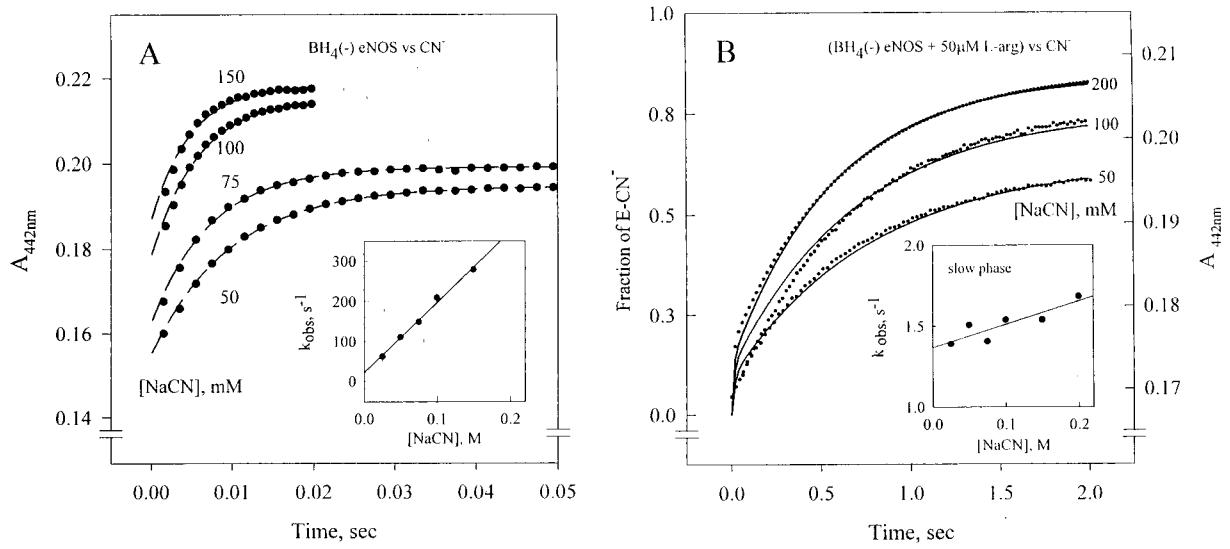

FIGURE 5: Kinetics of $BH_4(-)$ eNOS with cyanide. (A) eNOS at 2 μM was reacting with different concentrations of cyanide (numbers next to each kinetic curve) at 22 °C. Kinetic data acquired as $A_{442\ nm}$ changes (closed circles) fit to single-exponential function (dash lines) to obtain the observed rate constants. Inset: secondary plot to determine binding rate constants for cyanide ligand. (B) Kinetics of L-arginine preincubated $BH_4(-)$ eNOS with cyanide. Concentration of L-arginine was 50 μM, and cyanide levels are indicated next to each kinetic curve. Solid lines are computer simulations based on the same model used in Figure 4. Inset: secondary plot for the slow phase kinetics. Numbers next to each line are the millimolar concentrations of cyanide.

(12 mM), and is also much larger than that obtained from static titration methods (15.2 mM) (Figure 3B and Table 2).

To resolve the apparent contradiction, computer simulations based on model B was again conducted and successfully fit the observed kinetic data of $BH_4(-)$ eNOS, both the biphasic behavior and the observed rates. In the absence of L-arginine, the values for k_2 and k_{-2} obtained by direct exponential fits (1.8×10^3 M^{-1} s^{-1} and 22 s^{-1}, respectively) match closely those obtained by optimal simulation (2.0×10^3 M^{-1} s^{-1} and 22 s^{-1}, respectively) (Table 2). In the presence of L-arginine, the optimal values for k_3 and k_{-3} (5.0 M^{-1} s^{-1} and 0.2 s^{-1}, respectively) are ~400 and 110 times those of k_2 and k_{-2}, respectively, but the calculated K_d based on simulations, 40 mM, is much closer to that obtained from equilibrium titration (15.2 mM) than that obtained from secondary plot analysis (1.03 M). These results strongly indicate that L-arginine also decreases the "on" and "off" rate of cyanide binding to $BH_4(-)$ eNOS via an obstruction mechanism. Further, the biphasic kinetics (Figure 5B) are not due to heme heterogeneity but are simply the consequence of two populations of eNOS molecules that are either L-arginine-free or bound. The L-arginine-free eNOS molecules are proposed to bind cyanide with a nonobstructed rate (the fast phase in Figure 5B). Apparently L-arginine, at 50 μM, does not saturate all binding sites in $BH_4(-)$ eNOS. This implication of a lower L-arginine affinity in $BH_4(-)$ eNOS than $BH_4(+)$ eNOS also supports the notion that BH_4 enhances L-arginine binding, corroborating the results of

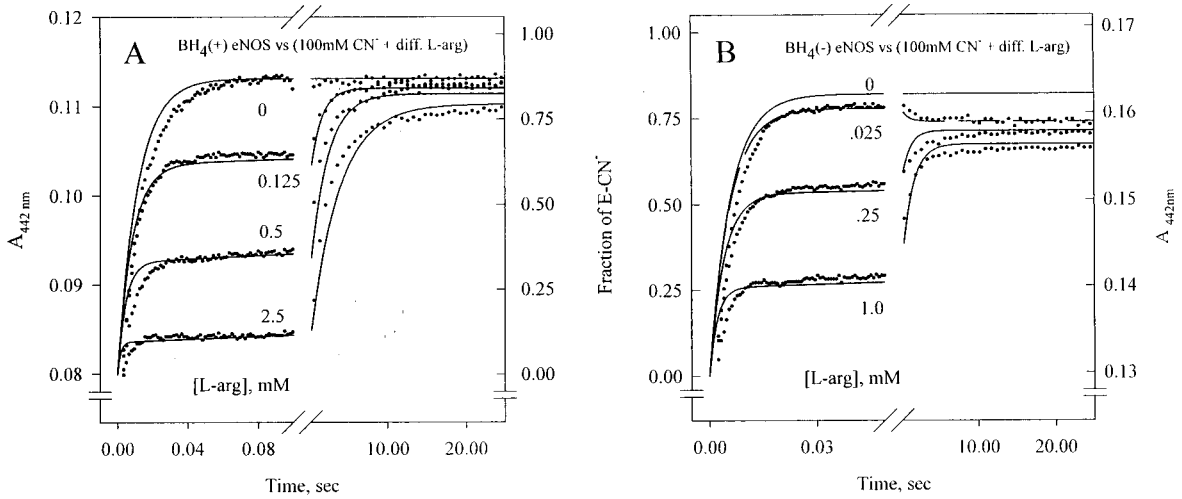

FIGURE 6: Kinetics of eNOS binding with a mixture containing 100 mM CN^- and different levels of L-arginine. (A) Kinetics of $BH_4(+)$ eNOS (2 μM) reacting with mixtures containing 100 mM cyanide and different amounts of L-arginine (dots). Lines are computer simulations based on the model B in Scheme 1 and rate constants listed in Table 2. (B) Kinetics of 2 μM $BH_4(-)$ eNOS reaction with a mixture of 100 mM cyanide and different amount of L-arginine (dots). Lines are computer simulations using rate constant values shown in Table 2. Numbers next to each traces in panels A and B are the concentrations of L-arginine.

static titration of cyanide binding (Figure 3, panel A vs panel B).

To evaluate the effect of L-arginine concentration, cyanide binding kinetics was further determined under another set of conditions. $BH_4(+)$ eNOS (Figure 6A) or $BH_4(-)$ eNOS (Figure 6B) were each reacted with a mixture containing 100 mM cyanide and varying amounts of L-arginine, ranging from 0 to 2.5 mM, in the stopped-flow apparatus. Multiphasic kinetics are observed for both eNOS samples under the same experimental conditions (Figure 6). The kinetic traces obtained using baculovirus-expressed eNOS can be fit by two exponentials, but the data on bacterial eNOS sample cannot be fit similarly because the absorbance changes change directions during the binding process (e.g., see the bimodal kinetic data obtained for reactions with 25 μM L-arginine shown in Figure 6B). It is noted that the total observed changes at $A_{442\ nm}$ due to cyanide binding is almost independent of L-arginine concentration. The overall effect of L-arginine is a concentration-dependent change in the proportions of the fast and slow components. With an apparent shift from the fast to slow component with increasing levels of L-arginine in the reaction.

Computer simulations based on model B were carried out to test its validity in interpreting the data of Figure 6. To our delight, the same set of parameter values used in fitting the data of Figures 4 and 5 also successfully simulate the multiphasic kinetic data in Figure 6. The simulations were not only remarkable in providing very similar rates and extent but also predicted the changes in the direction of the observed absorbance change. The agreement gives several important implications. The higher the concentration of L-arginine, the more efficient is its obstruction of cyanide binding, a consequence of faster L-arginine binding. The similar final level of cyanide binding suggest nonoverlapping binding sites for L-arginine and cyanide, a result supported by equilibrium binding data (Figure 3). The multiphasic binding kinetics is not due to heterogeneity of eNOS because the proportion of the different phases is regulated by the level of L-arginine. Changes in the direction of absorbance at 442 nm (Figure 6B) is a consequence of the difference in the rates of approach to equilibrium for L-arginine and cyanide and also further supports its lower L-arginine affinity for $BH_4(-)$ than the $BH_4(+)$ eNOS.

It is worth mentioning that the apparent binding rates at 100 mM cyanide and 25 μM L-arginine shown in Figure 6 as compared to those in Figures 4B and 5B are significantly larger. This difference in observed rates is the result of different experimental conditions. In the latter case, the binding equilibrium of L-arginine was first established before cyanide addition, whereas in the former case, both ligands are introduced simultaneously. The obstruction of cyanide binding shown in Figures 4B and 5B appeared to be more pronounced because L-arginine binding had already reached equilibrium.

Effect of L-Arginine and BH_4 on the NO Binding to eNOS. Under pseudo-first-order conditions, NO binding kinetics of baculovirus-expressed eNOS is monoexponential (Figure 7A). The k_{on} and k_{off} obtained from the secondary plot of k_{obs} vs NO concentration were 3.3×10^6 M^{-1} s^{-1} and 39 s^{-1}, respectively (Figure 7B). In contrast, in the presence of a saturating amount of L-arginine (50 μM), the kinetics of NO binding became heterogeneous (Figure 7B). Individual kinetic traces fit reasonably well to a two-exponential function with the fast phase contributing about 70% of the total observed changes. The on and off rate constants for both phases were analyzed by the secondary plot of k_{obs} vs NO concentrations. For the fast component, a k_{on} of 3.3×10^6 M^{-1} s^{-1} and a k_{off} of 35 s^{-1} were estimated, and a K_d of 10.6 μM was obtained (Figure 7C). These three values are very close to those obtained for the control (zero L-arginine). Similar results were obtained at three different L-arginine concentrations: 12.5, 25, and 50 μM (Figure 7C, three additional symbols). A k_{off} of 1.5 s^{-1} was similarly obtained for the slow phase of the reaction containing 25 μM L-arginine from the secondary plot, but the on rate could not be determined due to the negative slope (Figure 7B, inset), implying a rather small rate.

These kinetic data are best simulated as a 1:1 mixture with one heme center showing a standard NO binding reaction and the second heme follows a binding obstruction mecha-

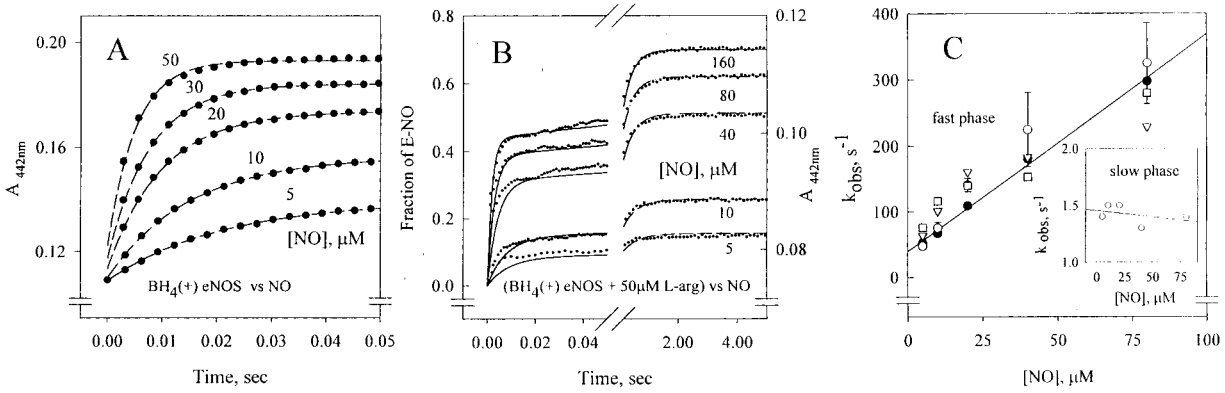

FIGURE 7: Kinetics of NO binding to ferric $BH_4(+)$ eNOS and $BH_4(+)$ eNOS preincubated with L-arginine, respectively. Anaerobic buffer containing 2 μM ferric baculovirus eNOS was mixed in the stopped-flow apparatus with anaerobic buffer containing NO at 23 °C. (A) $BH_4(+)$ eNOS at 2 μM was reacted with various levels of NO, and its kinetics was monitored by $A_{442\ nm}$ changes. Numbers next to each lines show concentrations of NO. Closed circles are the data, and the dash lines are single-exponential fits. (B) NO binding kinetics of 2 μM eNOS preincubated with 50 μM of L-arginine (dots). Solid lines are computer simulations using an adjusted model B and parameter values listed in Table 2 as detailed in the text. **(**C**)** Secondary plots of the observed rates obtained at various NO concentrations in the presence of 0 (closed circles), 12.5 (open circles), 25 (open squares), and 50 μM (open triangles) L-arginine. Inset: secondary plot of the 2nd (slow) phase reaction with NO of eNOS preincubated with 50 μM of L-arginine. For clarity, only part of the kinetic traces and simulations are presented in A and B panels.

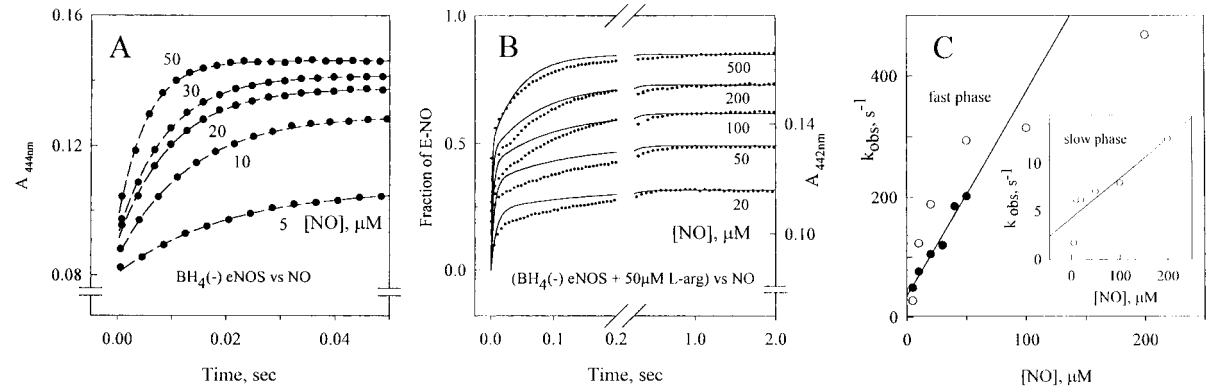

FIGURE 8: Kinetics of NO binding to $BH_4(-)$ eNOS and $BH_4(-)$ eNOS preincubated with L-arginine. (A) NO binding kinetics of 2 μM $BH_4(-)$ eNOS was monitored at $A_{442\ nm}$ at 23 °C. Numbers next to each line are concentrations of NO. Filled circles are the data, and the dash lines are the one-exponential fits. (B) NO binding kinetics of 2 μM eNOS preincubated with 50 μM of L-arginine (dots). Solid lines are computer simulations to the modified model B and parameter values listed in Table 2 as detailed in the text. (C) Secondary plots of the observed rates obtained at various NO concentrations in the absence (closed circles) and the fast phase kinetics in the presence of 50 μM of L-arg (open circles). Inset: secondary plot of the second (slow) phase NO binding reaction of eNOS preincubated with 50 μM of L-arginine. For clarity, only part of the kinetic traces and simulations are presented in A and B panels.

nism by L-arginine. As shown in Figure 7B and Table 2, simulations including a fast phase of 50% overall contribution with a k_{on} of 3×10^6 M^{-1} s^{-1} and a k_{off} of 33 s^{-1} and a slow phase with a k_{on} of 1×10^3 M^{-1} s^{-1} and a k_{off} of 1.5 s^{-1} match well with the observed kinetic data (Figure 7B). The calculated K_d from the simulations for the fast component is thus 11 μM, and K_d for the slow component is 1.5 mM, it is not possible to determine the latter from the secondary plot (Figure 7C, inset). This mechanism implies that the two heme centers in the eNOS dimer are different and L-arginine binding reveals subtle differences between these two heme centers. In contrast to the cyanide binding data, L-arginine showed a sizable effect on the plateau of the NO−eNOS complex, while the final level of the eNOS−cyanide complex is rather insensitive to the L-arginine concentration. The amount of NO−eNOS complex formation was verified by rapid-scan diode array, and it was confirmed that L-arginine binding significantly changed the binding affinity and thus the end point of NO binding to the ferric heme in both eNOS samples (Figure 7B).

E. coli-expressed eNOS (BH_4-deficient) also exhibited homogeneous NO binding kinetics (Figure 8A) with an estimated k_{on} of 3.4×10^6 M^{-1} s^{-1} and a k_{off} of 35 s^{-1} (Figure 8C). K_d was then calculated to be 10.3 μM. All three values are similar to those obtained for BH_4-abundant eNOS, indicating lack of an effect from BH_4 on NO binding to the ferric heme. On the other hand, pretreatment of eNOS with 50 μM L-arginine resulted in biphasic NO binding kinetics (Figure 8B). The fast phase accounts for 60% of the total observed optical change at 444 nm and had an association rate constant of 3.3×10^6 M^{-1} s^{-1} and a dissociation rate constant of 35 s^{-1} (Figure 8C and Table 2). These two values and the calculated K_d, 10.6 μM, are very close to the control. The slow phase that accounted for 40% of the total optical changes showed a k_{on} of 4.1×10^4 M^{-1} s^{-1} and a k_{off} of 4.3 s^{-1} (Figure 8C, inset). The on rate constant is 2 orders of magnitude slower than that of the fast phase, but the off rate constant is decreased by only 1 order of magnitude, thus leading to a K_d of 104 μM, 10 times larger than the fast phase (Table 2).

Similar to the BH_4(+) eNOS, computer simulations containing a fast phase with 50% overall contribution, a k_{on} of 2×10^6 M^{-1} s^{-1} and a k_{off} of 40 s^{-1}, and a slow phase with a k_{on} of 3×10^4 M^{-1} s^{-1} and a k_{off} of 6.3 s^{-1} nicely fit the observed kinetic data (Figure 8B). The calculated K_d for the fast phase is thus 20 μM, and the value for the slow phase is 210 μM. These K_d values are quite close to those values calculated from the ratio of the observed on and off rate constants obtained directly from the secondary plot (Table 2).

Thus, BH_4 did not show a significant effect on the NO binding to eNOS, as reflected by the lack of changes of the rate constants of the plain eNOS samples and the fast phase component of L-arginine-treated eNOS either BH_4(−) or BH_4(+) (Table 2). However, the slow phase component of the BH_4(+) eNOS appears to be more sensitive to L-arginine binding than that of BH_4(−) eNOS (Table 2).

Again, in the presence of L-arginine, the final level of NO-ferric NOS is dependent on the NO concentration and failed to plateau at NO concentrations that saturated the control eNOS. This indication of a shift of NO affinity in the slow component was further confirmed by rapid-scan diode array stopped-flow which showed that L-arginine indeed changed the affinity of the NO for both eNOS preparations (data not shown).

DISCUSSION

We have prepared eNOS with a full complement of heme, FAD, and FMN. By replenishing hemin and sepiapterin during cell growth, the BH_4 content can be raised to 0.7. With this eNOS preparation, we could undertake the experiments in which the stoichiometry of these cofactors is critical for data interpretation. To study the ligand binding kinetics, we need a homogeneous preparation to avoid possible heterogeneous kinetic data. We accomplished this for the heme and flavin groups of eNOS but are still unable to reconstitute BH_4 to a stoichiometric level. With stoichiometric amounts of heme, it is possible to define the heme extinction coefficient and thus the absorption coefficient of different ligand−heme complexes. This facilitates assessing the expected end point of binding equilibrium in static titrations and stopped-flow kinetic measurements. This will be critical for future characterization of electron-transfer mechanism. To evaluate the effect of BH_4, we chose to compare BH_4-deficient *E. coli*-expressed eNOS and BH_4-abundant eNOS (either baculovirus-expressed eNOS or *E. coli*-expressed eNOS reconstituted with BH_4), rather than adding excess exogenous BH_4, thus minimizing two potential problems:

(i) We may treat BH_4 as a cofactor if we have only protein-bound BH_4. With excess exogenous BH_4, this component will serve dual roles, both as a ligand and a cofactor. Most of our experiments to evaluate the effect of L-arginine on small heme ligand binding already have two ligands in the binding system. Introducing another free ligand, BH_4, will further complicate data analysis.

(ii) Free BH_4 molecules autoxidize rapidly in the buffer systems commonly used for NOS samples (*33*; and our unpublished data). With excess exogenous BH_4, we face a heterogeneous population of biopterin present at different redox states with the concentration of BH_4 at each redox state constantly changing during the experiments.

To control the autoxidation of BH_4 and to achieve a homogeneous system for the binding reaction, we decided to use eNOS samples that are either free of BH_4 [BH_4(−) eNOS] or specifically reconstituted to the eNOS protein [BH_4(+) eNOS]. Excess exogenous BH_4 used to reconstitute *E. coli*-expressed eNOS has been removed by gel filtration.

Imidazole and L-arginine binding to eNOS were demonstrated previously to be mutually exclusive (*9*). Depending on how the experiments are executed, the kinetic data can take a very different appearance, as illustrated in Figures 1 and 2. The data with simple exponential kinetics was easily fit by model A (Scheme 1) using the previously measured on and off rate constants for both ligands (*9*) (Figure 1, panels B and D). Kinetic data obtained for BH_4(+) and BH_4(−) eNOS were conspicuously biphasic (Figure 2, panels A and B) but are also fit to model A using the same set of rate constants that optimally fit the data in Figure 1 (lines in Figure 2). Our simulations not only validate the simple competition model but also demonstrate that the influence of BH_4 on the interaction between L-arginine and imidazole is minimal.

In contrast, L-arginine substantially reduced the rates of cyanide binding on both the association and dissociation steps in eNOS samples whether BH_4 was present or not (Figures 4−6). This sizable decline in apparent binding rates is not due to the crowding of the ligand access channel, because binding of cyanide is not influenced by weakly associated, but bulkier, type II ligands such as histamine and nicotinic acid (data not shown). The simple obstruction model listed in Scheme 1, model B successfully simulated all our cyanide binding data (compare Figures 4−6) by decreasing the values of k_2 and k_{-2} to k_3 and k_{-3} when L-arginine is present. The modeling closely simulates the observed rates, extent, and also the multiphasic kinetics with opposite absorbance changes as manifested by the data (Figure 6B, see the data for 25 and 50 μM L-arginine). Because the cyanide binding kinetics was measured at one fixed L-arginine concentration (Figures 4 and 5) or increasing levels of L-arginine (Figure 6), a single set of values capable of fitting all the kinetic data attest to the correctness of the model.

This obstruction model is also coincident with the recent 3-D structure of the eNOS oxygenase domain (*6*, *7*), containing an L-arginine sitting right on top of the heme moiety and able to impede cyanide ligation to and dissociation from the heme iron. The distance between the arginino nitrogen and the heme iron defined by X-ray crystallography and ENDOR study, 4.05 Å (*34*), is larger than the space required for a cyanide ligand, ∼3 Å. (∼1.9 Å between Fe and C and ∼1.1 Å for the C≡N bond) (*35*). On the other hand, with cyanide bound to the heme iron should not influence the L-arginine binding kinetics, as corroborated by the same rate constants, k_1 and k_{-1}, used in Scheme 1, eq B4.

In the presence of L-arginine, both kinetics of imidazole and cyanide binding show an initial jump of binding to BH_4(−) eNOS as compared to BH_4(+) eNOS (Figure 2, panels B vs A, and Figure 5B vs Figure 4B). This difference is due to the lower L-arginine binding affinity for BH_4(−) eNOS than to BH_4(+) eNOS, so the former has a larger fast phase to the L-arginine-free eNOS protein. To simulate the kinetics properly, a K_d value of ∼5.0 μM for L-arginine was used for BH_4(−) eNOS and 1.0 μM was used for BH_4(+)

eNOS. These results corroborate a previous observation that BH_4 binding enhances the L-arginine binding (*36*). Furthermore, the subtle difference in the equilibrium cyanide binding between $BH_4(+)$ and $BH_4(-)$ eNOS substantiate the effect of BH_4 in enhancing the heme ligand binding. Thus, the heme, BH_4, and L-arginine "triad" enhance one another to achieve a stable and rigid "scaffold". Such rigid orientation is essential for efficient oxygen activation and NO formation chemistry. The absence of BH_4 or L-arginine or both in the heme distal region results in a "wobbling" heme, leading to a slow on rate or faster off rate constant for heme ligands. This concept is supported by X-ray data, which show extensive direct and indirect hydrogen-bonding interactions between L-arginine and heme and between heme and BH_4 (*5*−*7*).

It is noteworthy that in the presence of L-arginine, the apparent K_d calculated from secondary plots, 1.03 and 0.5 M for $BH_4(-)$ and $BH_4(+)$ eNOS are substantially larger than those calculated as k_{-3}/k_3 from numerical integration, i.e., 40 and 30 mM, respectively, and those equilibrium constants obtained by optical titrations, i.e., 15.2 and 15.1 mM, respectively (Table 2). The similar ending points of the stopped-flow kinetic data shown in Figure 6 also indicate that cyanide binding affinity was little affected by L-arginine. This discrepancy is not due to the data scatter for the low values of measured rate of L-arginine-treated eNOS. The linearity of the data measured in the presence and absence of L-arginine is very similar with $r^2 > 0.99$. This result indicates that the apparent k_{on} and k_{off} obtained from the secondary plot cannot be used to define the ligand affinity in our binding experiments that involve multiple ligands. Computer simulation or fitting to a reliable mechanistic model is essential to get optimal values for the rate and equilibrium constants.

Kinetic data of NO binding are more complicated. Both $BH_4(+)$ and $BH_4(-)$ ferric eNOS exhibited standard homogeneous second-order binding kinetics (Figure 7A and 8A). However, addition of L-arginine appeared to separate each eNOS sample into two different populations with one part remaining insensitive to L-arginine binding but the other part showing substantially reduced rates. Although we succeeded in interpreting the NO binding data using an extended obstruction model, other binding models might explain the same data. However, the simple model that L-arginine binding resulted in a significant "partial obstruction" of NO binding association and dissociation provides a remarkably simple interpretation for the L-arginine-insensitive fast binding phase and the L-arginine sensitive slow phase both in their rates and extent.

The implication for structural differences between the two heme centers in the NOS dimer is not apparent from the recent X-ray crystallographic data (*7*). However, our earlier EPR study of the low-spin heme complexes of imidazole and its analogues clearly showed heterogeneous heme rhombicity (*37*). In addition, more than one ferrous heme−CO structures are revealed by rR studies (*21*). The possible existence of a structural difference between the two heme centers in eNOS was only apparent after the introduction of L-arginine in our kinetic measurements, indicating these changes are subtle and not disclosed by X-ray crystallography. The significance of this heme perturbation in terms of catalysis is yet to be defined. The L-arginine effect on NO binding kinetics corroborates our recent study of the geminate rebinding of NO (*38*). In the presence of L-arginine, the multiphasic rebinding of NO after the laser flash shifts to a slower rate as compared to the control and also the contribution of each phase is changed sizably. It was proposed that L-arginine binding resulted in a larger activation barrier for those NO ligands that escaped out of the heme pocket to overcome for the reassociation process. Such a kinetic barrier is likely to be the result of the physical location of the bound L-arginine relative to the heme plane as disclosed by the X-ray crystallographic data (*5*−*7*). Such a barrier should slow both the binding and the dissociation of NO as observed in our stopped-flow measurements.

Abu-Soud et al. have measured NO kinetic binding to the ferric iNOS and evaluated the effect of both L-arginine and BH_4 on the NO binding (*15*). Their results indicate that neither BH_4 nor L-arginine showed a significant effect. The rate constants they obtained are comparable with our control $BH_4(+)$ and $BH_4(-)$ eNOS data. The insensitivity to BH_4 of NO binding to iNOS is similar to eNOS. However, the lack of effect from L-arginine is in sharp contrast to our data. The structure in the heme pocket that contains the BH_4 and L-arginine groups are essentially superimposable between eNOS and iNOS based on the X-ray data (*2*, *7*). It is not clear why the NO binding kinetics showed a large difference in L-arginine sensitivity between iNOS and eNOS, although the experiments were carried out at somewhat different conditions. The main difference is that Abu-Soud et al. used an excess exogenous BH_4 to evaluate the BH_4 effect, thus BH_4 was both a ligand and a cofactor (*15*). Recent geminate rebinding kinetics between NO and ferric nNOS also showed monophasic binding kinetics and no dependence on either L-arginine or BH_4 (*18*). Although the binding affinity and kinetics of L-arginine-free NOS are very similar for all three isoforms (*15*, *18*; and this study), L-arginine only caused significant changes in the NO binding kinetic behavior of eNOS. This is another selective effect observed so far for this substrate.

Although NO and cyanide are isoelectronic and similar in molecular size, their binding kinetics and the response to L-arginine are quite different. The substantially reduced affinity for heme of anionic cyanide than NO is likely be the result of the stronger negative trans effect from the thiolate heme ligand. This additional charge probably also plays a role in the stronger obstruction in heme binding by L-arginine as the electrostatic interaction between the cationic arginino headgroup and the cyanide anion should be much stronger than that with NO, thus leading to slower k_{on} and k_{off} for cyanide. It is not clear why L-arginine distinguished the two heme populations in the eNOS−NO complex but not in the cyanide−heme complex. The ability of NO but not cyanide to adopt either a linear (sp hybridization) or bent (sp2 hybridization) conformation may explain its different sensitivity to the L-arginine binding than cyanide. Further characterization is needed to test this proposal.

In summary, an eNOS preparation with a full complement of heme and flavins was used to evaluate the intricate interactions among the heme, L-arginine, and BH_4 triad using three small heme ligands; each exhibited distinctive binding behavior to eNOS. This study is first in which BH_4 was treated solely as a cofactor and not a ligand. In addition, for the first time, discrete mechanistic models were developed

to successfully interpret the binding mechanism. Imidazole is strictly competitive with L-arginine, but the binding of cyanide and NO are very differently affected by L-arginine. An obstruction model was successfully applied to fit all the kinetic data. BH_4 showed only an indirect effect by strengthening the "triad" scaffolding. Potential pitfalls in analyzing kinetic data derived from multiple ligand interactions and using a secondary plot between the k_{obs} and ligand concentrations are well-exemplified by the cyanide binding kinetics. It is thus critical to resolve the ligand binding mechanism using computer modeling. Implication of two different heme centers in the eNOS dimer was also provided by the NO binding data, which is in sharp contrast with other NOS isozymes. This subtle difference has yet to be revealed by the X-ray crystallography.

ACKNOWLEDGMENT

We want to thank Drs. Pavel Martásek and Beattie Sue Siler Masters for their generous gift of the *E. coli* expression system for bovine eNOS. We also are grateful to Drs. Bettie Sue Siler Masters, Bernd Mayers, Paul R. Ortiz de Montellano, and Dennis J. Stuehr for their NOS samples; Dr. Julian Peterson for his $P450_{BM3}$, and Dr. Henry Strobel for his $P450_{1A1}$ used in our heme and tryptophan analysis. We also thank Drs. Graham Palmer and Richard Kulmacz for careful reading of the manuscript.

REFERENCES

1. Feldman, P. L., Griffith, O. W., and Stuehr, D. J. (1993) *Chem. Eng. News 51*, 26−38.
2. Raman, C. S., Martásek, P., and Masters, B. S. S. (2000) in *The Phorphyrin Handbook* (Kadish, K. M., Smith, K. M., and Guilard, R., Ed.) pp 293−339, Academic Press.
3. Masters, B. S. S., McMillan, K., Sheta, E. A., Nishimura, J. S., Roman, L. J., and Martásek, P. (1996) *FASEB J. 298*, 249−258.
4. Stuehr, D. J. (1999) *Biochim. Biophys. Acta 1411*, 217−230.
5. Crane, B. R., Arvai, A. S., Ghosh, D. K., Wu, C., Getzoff, E. D., Stuehr, D. J., and Tainer, J. A. (1998) *Science 279*, 2121−2126.
6. Raman, C. S., Li, H., Martásek, P., Král, V., Masters, B. S. S., and Poulos, T. L. (1998) *Cell 95*, 1−20.
7. Fischmann, T. O., Hruza, A., Xiao, D. N., Fossetta, J. D., Lunn, C. A., Dolphin, E., Prongay, A. J., Reichert, P., Lundell, D. J., Narula, S. K., and Weber, P. C. (1999) *Nat. Struct. Biol. 6*, 233−242.
8. Matsuoka, A., Stuehr, D. J., Olson, J. S., Clark, P., and Ikeda-Saito, M. (1994) *J. Biol. Chem. 269*, 20335−20339.
9. Berka, V., Chen, P.-F., and Tsai, A.-L. (1996) *J. Biol. Chem. 271*, 33293−33300.
10. Wolff, D. J., Datto, G. A., Samatovicz, R. A., and Tempsick, R. A. (1993) *J. Biol. Chem. 268*, 9425−9429.
11. McMillan, K., and Masters, B. S. S. (1993) *Biochemistry 32*, 9875−9880.
12. Roman, L. J., Sheta, E. A., Martásek, P., Gross, S. S., Liu, Q., and Masters, B. S. S. (1995) *Proc. Natl. Acad. Sci. U.S.A. 92*, 8428−8432.
13. Chabin, R. M., McCauley, E., Calaycay, J. R., Kelly, T. M., MacNaul, K. L., Wolfe, G. C., Hutchinson, N. I., Madhusudanaraju, S., Schmidt, J. A., Kozarich, J. W., and Wong, K. K. (1996) *Biochemistry 35*, 9567−9575.
14. Abu-Soud, H. M., Gachhui, R., Raushel, F. M., and Stuehr, D. J. (1997) *J. Biol. Chem. 272*, 17349−17353.
15. Abu-Soud, H. M., Wu, C., Ghosh, D. K., and Stuehr, D. J. (1998) *J. Biol. Chem. 37*, 3777−3786.
16. Sato, H., Sagami, I., Daff, S., and Shimizu, T. (1998) *Biochem. Biophys. Res. Commun. 253*, 845−849.
17. Sato, H., Nomura, S., Sagami, I., Ito, O., Daff, S., and Shimizu, T. (1998) *FEBS Lett. 430*, 377−380.
18. Scheele, J. S., Bruner, E., Kharitonov, V. G., Martásek, P., Roman, L. J., Masters, B. S. S., Sharma, V. S., and Magde, D. (1999) *J. Biol. Chem. 274*, 13105−13110.
19. Scheele, J. S., Kharitonov, V. G., Martásek, P., Roman, L. J., Sharma, V. S., Masters, B. S. S., and Magde, D. (1997) *J. Biol. Chem. 272*, 12523−12528.
20. Tetreau, C., Tourbez, M., Gorren, A., Mayer, B., and Lavalette, D. (1999) *Biochemistry 38*, 7210−7218.
21. Wang, J., Stuehr, D. J., and Rousseau, D. L. (1997) *Biochemistry 36*, 4595−4606.
22. Chen, P.-F., Tsai, A.-L., Berka, V., and Wu, K. K. (1996) *J. Biol. Chem. 271*, 14631−14635.
23. Chen, P.-F., Tsai, A.-L., and Wu, K. K. (1994) *J. Biol. Chem. 269*, 25062−25066.
24. Chen, P.-F., Tsai, A.-L., and Wu, K. K. (1995) *Biochem. Biophys. Res. Commun. 215*, 1119−1129.
25. Martásek, P., Liu, Q., Liu, J., Roman, L. J., Gross, S. S., Sessa, W. C., and Masters, B. S. S. (1996) *Biochem. Biophys. Res. Commun. 219*, 359−365.
26. Smith, P. K., Krohn, R. I., Hermanson, G. T., Mallia, A. K., Gartner, F. H., Provenzano, M. D., Fujimoto, E. K., Goeke, N. M., Olson, B. J., and Klenk, D. C. (1985) *Anal. Biochem. 150*, 76−85.
27. Peterson, G. L. (1977) *Anal. Biochem. 83*, 346−356.
28. Holmquist, B., and Vallee, B. L. (1973) *Biochemistry 12*, 4409−4417.
29. Berry, E. A., and Trumpower, B. L. (1987) *Anal. Biochem. 161*, 1−15.
30. Rodriguez-Crespo, I., Gerber, N. C., and Ortiz de Montellano, P. R. (1996) *J. Biol. Chem. 271*, 11462−11467.
31. Stuehr, D. J., and Ikeda-Saito, M. (1992) *J. Biol. Chem. 267*, 20547−20550.
32. Sono, M., Stuehr, D. J., Ikeda-Saito, M., and Dawson, J. H. (1995) *J. Biol. Chem. 270*, 19943−19948.
33. Blair, J. A., and Pearson, A. J. (1973) *J. Chem. Soc., Perkin Trans. 2*, 80−88.
34. Tierney, D. L., Martásek, P., Doan, P. E., Masters, B. S. S., and Hoffman, B. M. (1998) *J. Am. Chem. Soc. 120*, 2983−2984.
35. Yu, N.-T. (1986) *Methods Enzymol. 130*, 351−409.
36. Klatt, P., Schmidt, M., Leopold, E., Schmidt, K., Werner, E. R., and Mayer, B. (1994) *J. Biol. Chem. 269*, 13861−13866.
37. Tsai, A.-L., Berka, V., Chen, P,-F., and Palmer, G. (1996) *J. Biol. Chem. 271*, 32563−32571.
38. Négrerie, M., Berka, V., Vos, M. H., Liebl, U., Lambry, J.-C., Tsai, A.-L., and Martin, J.-L. (1999) *J. Biol. Chem. 274*, 24694−24702.

BI992769Y